

Microstructure Evolution of Cold-Sprayed Al-Si Alloy Coatings on γ -TiAl During Heat Treatment

Jiqiang Wang, Lingyan Kong, Tiefan Li, and Tianying Xiong

(Submitted March 11, 2015; in revised form May 26, 2015)

This paper investigated the influence of heat treatment on the microstructure of Al-Si alloy coatings on γ -TiAl alloy. The coatings were prepared by cold spraying with Al-12Si and Al-20Si alloy powders as the feedstock, and then the as-sprayed coatings were subjected to heat treatment. The microstructure, chemical composition, and phase transformation of the coatings were studied by SEM, XRD, and EPMA. The diffusing behavior of Al and Si during heat treatment was investigated. The results showed that a silicon-aluminizing coating was formed through the inward diffusion of Al/Si elements into the substrate. The obtained kinetics curve of the formation of silicon-aluminizing coating at 580 °C similarly followed parabolic law.

Keywords Al-Si alloy coating, cold spray, diffusing behavior, γ -TiAl alloy, heat treatment

1. Introduction

TiAl-based alloys exhibit great potential for high-temperature structural applications such as turbine blades of internal combustion engines, owing to their low density, high specific strength, and high creep resistance (Ref 1-3). However, the poor oxidation resistance at temperature above 800 °C and environmental embrittlement of γ -TiAl limit its application (Ref 4-6). Therefore, the γ -TiAl-based alloys should be protected in order to be used at elevated temperatures.

Usually, protective coatings which could form a slow-growing Al_2O_3 or SiO_2 scale were expected to improve the oxidation resistance of the alloys. Aluminide coatings had attracted many researchers' interests for its good compatibility with γ -TiAl substrate (Ref 6-11). Various methods to form the aluminide coatings on γ -TiAl substrate had been studied, including pack cementation (Ref 6, 7), sputtering aluminium and annealing (Ref 8), hot-dip coating (Ref 9), and cold-sprayed aluminum and annealing (Ref 10, 11). Besides the aluminide coatings, siliconizing coatings were also applied on γ -TiAl-based alloys. The results showed that an SiO_2 scale was formed on the siliconizing coatings during the oxidation test and thus improved the oxidation resistance of the bare alloys (Ref 12-14). Thus, taking into account the favorable effect of both elemental Al and Si on the improvement in the

oxidation resistance of γ -TiAl, co-deposition of Al and Si to form oxidation-resistant coatings might be a good choice. Several researches had investigated on the co-deposition of Al and Si on γ -TiAl alloy such as preparation of Al-Si diffusion coating by Arc-PVD by Swadzba (Ref 15), pack cementation by Al and Si by Xiang (Ref 16), and liquid siliconizing by Al-Si alloys by Xiong (Ref 17, 18). The results (Ref 15-18) showed that the Al-Si diffusion coating could improve the oxidation resistance of the bare alloy significantly.

Lately, cold spray developed widely as a notable technique for coating preparation. In the process, the temperature of the carrier gas and particles remains far below the melting point of the metal powders. So the particles are in the solid state as they hit the substrate and deposit on the substrate to form coatings through plastic deformation. Therefore, the coatings prepared by cold spray usually have low porosity, low oxide, and low residual stress (Ref 19-21).

In this paper, cold spray as a novel and convenient method was used to prepare Al-12Si and Al-20Si alloy coatings on γ -TiAl substrate. After the deposition, the as-sprayed coatings were subjected to heat treatment. The elements' diffusion and microstructure evolution of the coatings during the heat-treatment process were studied. The kinetics of the diffusion coating was also investigated.

2. Experimental

The nominal composition of the γ -TiAl substrate was Ti-47Al-2Cr-2Nb-0.15B (at.%), which was provided by Titanium Alloys Division, Institute of Metal Research, CAS. The ingot was cut into 15 mm \times 10 mm \times 2 mm coupons. The surface of all the specimens was ground with SiC paper up to 800 grit, cleaned ultrasonically in anhydrous alcohol, dried, and then pilled before cold spray.

Jiqiang Wang, Lingyan Kong, Tiefan Li, and Tianying Xiong, Institute of Metal Research, Chinese Academy of Sciences, Shenyang 110016, China. Contact e-mail: lykong@imr.ac.cn.

Commercial Al-12Si (wt.%) and Al-20Si (wt.%) alloy powders (by *Changsha Tianjiu* metallic materials Co., Ltd.) were used for cold spray. Before spray, both of the powders were dried at 80 °C for 4 h to remove the moisture. The cold spray device was manufactured by Institute of Metal Research, CAS. The De Laval nozzle was a rectangle exit equipped with a cross section of 2 mm × 10 mm and a throat of 2 mm × 2 mm. The parameters for the cold spray process are listed in Table 1.

The as-sprayed specimens were subjected to heat treatment in a tube furnace under argon gas flow of 40 mL/min. The heating rate was 3 °C/min. After the heat treatment, the furnace was then cooled to room temperature at its natural rate by switching off the power. At the beginning, three temperatures were used for the heat treatment: 530 °C, lower than the melting point of the Al-12Si and Al-20Si alloys; 580 °C, near the melting point; and 650 °C, higher than the melting point. However, no reaction or interdiffusion between the coating and substrate was observed after heat treatment at 530 °C. Thus

only the results of heat treatment at 580 and 650 °C were reported in the next work.

A mixture of 10 mL HF, 5 mL HNO₃, and 85 mL H₂O was used for etching the feedstock particles and as-sprayed coatings. The thickness of the silicon-aluminizing coating was measured using the SEM images. Every sample was measured at 20 different positions randomly, and the average thickness was adopted as the thickness of the coating.

X-ray diffraction (XRD) analysis was conducted on D/max-2500pc (RIGAKU, Japan). Scanning electron microscopy (SEM-EDS) imaging was obtained using JSM-6301F (SHIMADZU, Japan) and Inspect F50 (FEI, USA). The electron probe microanalysis was obtained using EPMA-1610 (SHIMADZU, Japan).

3. Results and Discussion

3.1 Characteristics of Al-12Si and Al-20Si Alloy Powders

Figure 1 shows the morphology and etching cross section of Al-12Si and Al-20Si alloy powders. It could be seen that both of the powder particles were nearly spherical. Because the composition of Al-12Si was similar with the eutectic composition of 12.7% Si in Al-Si system (Ref 22), the Al-12Si particle showed a microstructure resulting from eutectic reaction as shown in Fig. 1(b). The EDS results indicated that the dark gray phase was Al rich and

Table 1 Parameters for cold spray

Parameters	Al-12Si	Al-20Si
Main gas, air	2.0 Mpa	2.0 Mpa
Temperature	300 °C	360 °C
Standoff distance	15 mm	15 mm
Traveling speed of the gun	200 mm/min	200 mm/min

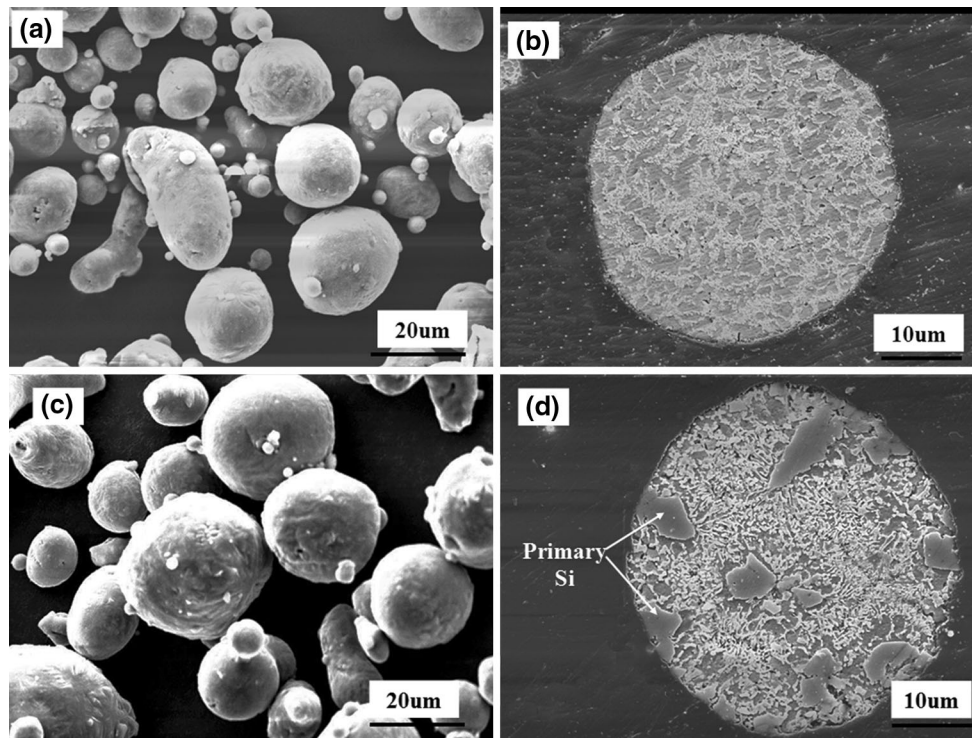


Fig. 1 Morphology of the (a) Al-12Si powders and (c) Al-20Si powders and the etched cross section of (b) Al-12Si particle and (d) Al-20Si particle

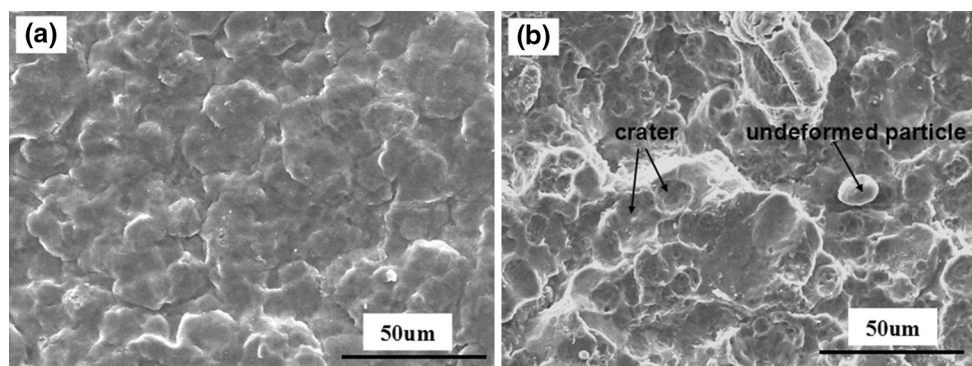


Fig. 2 Surface morphology of the as-sprayed (a) Al-12Si alloy coating and (b) Al-20Si alloy coating

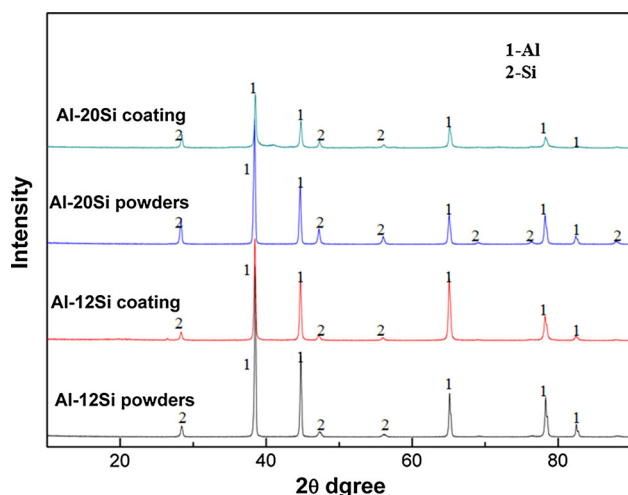


Fig. 3 XRD patterns of the Al-12Si and Al-20Si feedstocks and the as-sprayed Al-12Si and Al-20Si alloy coatings

the light gray phase was Si rich (Ref 23). From the etching cross section of Al-20Si alloy particle as shown in Fig. 1(d), the Al-20Si powder contained not only the eutectic structure but also primary silicon particles (Ref 24). This is because Al-20Si is hypereutectic alloy.

3.2 Microstructure of the As-sprayed Al-12Si and Al-20Si Alloy Coatings

Figure 2 shows the surface morphology of the as-sprayed Al-12Si and Al-20Si alloy coatings. From Fig. 2(a), it could be seen that the surface of Al-12Si alloy coating was squamous. All the particles were well flattened. Compared with the Al-12Si alloy coating, the surface of Al-20Si alloy coating was relatively rough as shown in Fig. 2(b). Many craters which were created by the rebound particles were observed (Ref 20, 25). Some undeformed particles were also observed on the surface of the coating. The different surface morphology between Al-12Si and Al-20Si alloy coating might result from the difference of their ductility. The ductility of Al-20Si particle was lower than that of Al-12Si particle because of the presence of primary Si in the Al-20Si alloy (Ref 24). Thus

the Al-20Si particles were more difficult to deform during cold spray process. This is also the reason that a higher temperature was used for spraying Al-20Si particles.

Figure 3 shows the XRD pattern of the feedstock powders and the as-sprayed coatings. It could be seen that the diffraction peaks of the as-sprayed coatings were similar to those of the feedstock powders. Both the as-sprayed coatings and feedstock powders were composed of silicon and aluminum phase. This result indicated that there was no observable oxidation or phase transformation during the cold spray process.

Figure 4 shows the cross section of the as-sprayed Al-12Si and Al-20Si alloy coatings. From Fig. 4(a), it could be seen that the Al-12Si coating was about 30 μm thick. It bonded well with the substrate. No significant pores or cracks were observed in the coating. From the etching cross section in Fig. 4(b), the structure of Al-12Si alloy coating was made up of highly deformed powder splats, which was in accordance with the well-flattened surface morphology of the coating. Some porosity could be observed within the coating. They were probably exaggerated by etching. In the splat, two phases could be distinguished clearly. The dark gray phase was Al rich and the light gray phase was Si rich according to the EDS analysis, which was the same as the structure of Al-12Si powder particle. It indicated that the structure of Al-12Si powder particle did not change during the cold spray process. From Fig. 4(c), it could be seen that the Al-20Si alloy coating was about 50 μm thick. It also had good adhesion to the substrate and was compact without visible pores. Figure 4(d) shows the etching cross section of Al-20Si alloy coating. Many less-deformed particles were observed in the coating. It indicated that the deformation degree of Al-20Si particle was lower than that of Al-12Si particle due to the lower ductility of Al-20Si alloy. The microstructure of the particle in the Al-20Si alloy coating was also similar to that of the Al-20Si feedstock particle.

From the above analysis, the as-sprayed coatings inherit the microstructure of feedstock particles without phase transformation and oxidation. This is mainly attributed to the low spray temperature. According to literature (Ref 23), the solution temperature for Al-12Si is about 504-516 $^{\circ}\text{C}$. The temperature of spraying Al-12Si in

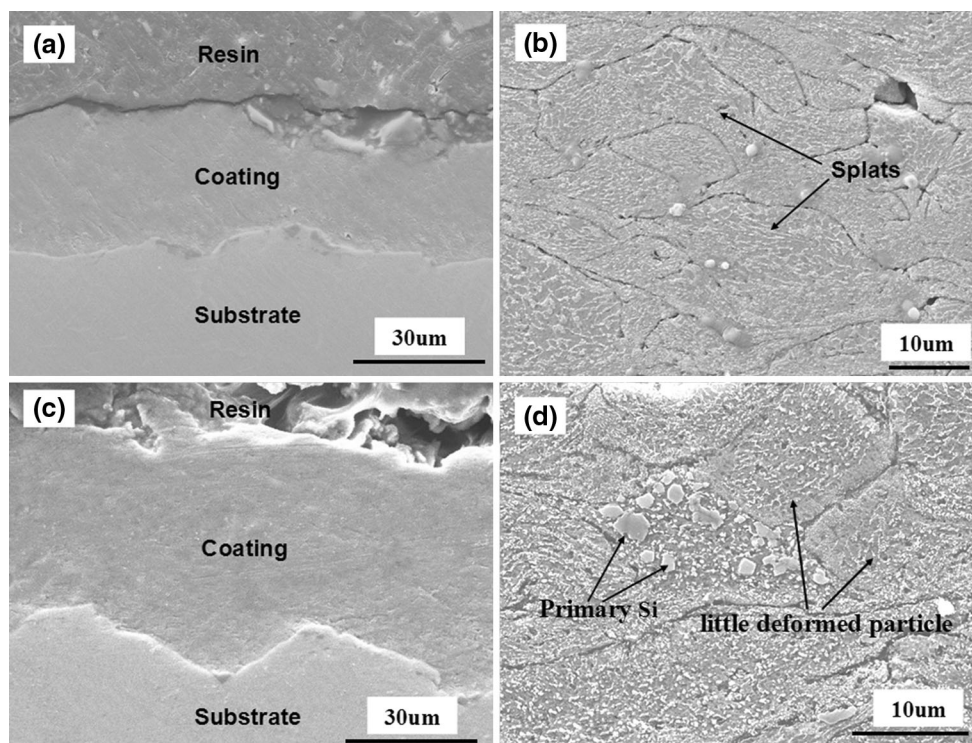


Fig. 4 Cross section of (a) the as-sprayed Al-12Si alloy coating, (b) the etched Al-12Si alloy coating, (c) the as-sprayed Al-20Si alloy coating, and (d) the etched Al-20Si alloy coating

this paper is 300 °C, far lower than the solution temperature. Therefore, the thermal effect on feedstock particles is very limited. The precipitation and growth of Si particles which were common in thermally sprayed Al-12Si coating do not occur during the cold spray process. The cold-sprayed Al-20Si is similar to Al-12Si. Therefore, when comparing to thermal spraying, low spray temperature is one main advantage of cold spraying.

3.3 Microstructure evolution of the coatings during heat treatment at 580 °C

Figure 5 shows the microstructure of Al-12Si alloy coating after heat treatment at 580 °C for 2, 4, 8, and 12 h. Table 2 shows the EDS analysis of different positions. From Fig. 5(a), it could be seen that a 4- μm -thick light gray interlayer was formed between the coating and the substrate. The interlayer was compact and crack free. Its chemical composition was 30.2 at.% Ti, 11.8 at.% Al, 55.3 at.% Si, and a small amount of Nb. According to the research on ternary Ti-Al-Si system (Ref 26, 27), this interlayer was identified as the ternary $\tau_2\text{-Ti}(\text{Al}_x\text{Si}_{1-x})_2$ phase with x in the range 0.15-0.3. The ternary τ_2 phase can also be written as AlSi_5Ti_3 according to the atomic ratio. Xiong et al. found that Si diffused strongly from the brazing alloy to the surface of TiAl when they used an Si-containing aluminum-based brazing alloy to join pure aluminum to the TiAl (Ref 28). In this paper, the formation of τ_2 interlayer also resulted from strongly inward diffusion of Si to the substrate, which could be indicated

by the lack of Si in the residual coating (position 1 in Fig. 5a, Table 2). Extending heat-treatment time to 4 h, the thickness of τ_2 interlayer increased to 7 μm as shown in Fig. 5(b). It indicated that Si continued to diffuse into $\gamma\text{-TiAl}$ substrate. Meanwhile, some Al-rich phases (position 2 in Fig. 5b, Table 2) appeared at the top of the interlayer, which might be formed by the inward diffusion of Al to the τ_2 interlayer.

After 8-h heat treatment as shown in Fig. 5(c), a dark gray layer was formed beneath the τ_2 interlayer. According to the chemical composition by the EDS analysis, this dark gray layer (position 4 in Fig. 5c, Table 2) was $\text{Ti}(\text{Al},\text{Si})_3$ whose Al atoms had been partly substituted by the Si atoms in the ordered lattice of TiAl_3 . It was reported that the solubility of Si in the TiAl_3 phase could reach up to 15 at.% (Ref 27). The chemical composition of the dark gray layer in this paper was in agreement with this result. One feasible mechanism of the formation of $\text{Ti}(\text{Al},\text{Si})_3$ layer was the rejection of Al into the substrate. During heat treatment, Si diffused into the substrate prior to Al element because Ti preferred to combine with Si rather than Al (Ref 17). This resulted in the formation of τ_2 phase with a low content of Al. Thus the excess Al in the original TiAl phase had to return to the τ_2/TiAl interface. This, in turn, resulted in the enrichment of Al in these areas and the localized transformation of TiAl into TiAl_2 and finally into TiAl_3 . The resulting τ_2/TiAl_3 equilibrium was transient due to the relatively rapid enrichment of silicon into the TiAl_3 . Finally, the $\text{Ti}(\text{Al},\text{Si})_3$ layer was formed beneath the τ_2 layer. Munro (Ref 14) reported

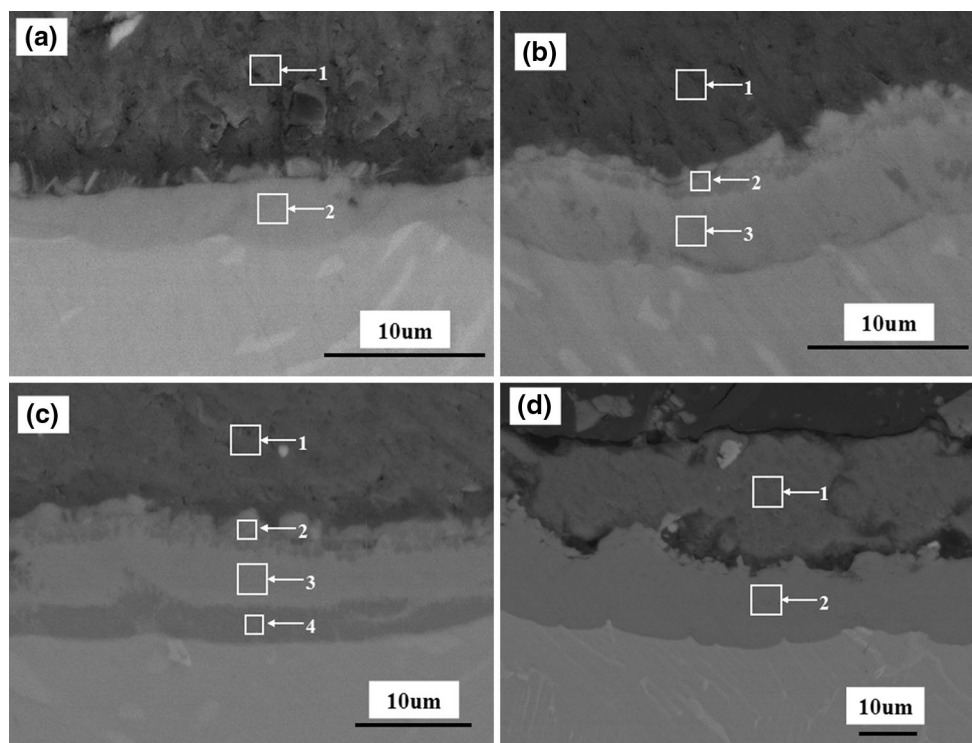


Fig. 5 Microstructure of the Al-12Si alloy coating after heat treatment at 580 °C for (a) 2 h, (b) 4 h, (c) 8 h, and (d) 12 h

Table 2 EDS analysis of different positions in Fig. 5 and 6

Position	Al, at. %	Ti, at. %	Si, at. %	Cr, at. %	Nb, at. %	Phase
1 in Fig.5(a)	99.8	0.2	Al
2 in Fig.5(a)	11.8	30.2	55.3	0.5	2.2	τ_2
1 in Fig.5(b)	99.8	0.2	Al
2 in Fig.5(b)	58.4	9.9	25.0	5.3	1.4	...
3 in Fig.5(b)	12.9	30.4	54.0	0.5	2.2	τ_2
1 in Fig.5(c)	99.7	0.3	Al
2 in Fig.5(c)	65.0	10.9	19.4	4.7
3 in Fig.5(c)	11.7	31.1	54.5	0.5	2.3	τ_2
4 in Fig.5(c)	57.4	25.1	15.1	0.6	1.8	Ti(Al,Si) ₃
1 in Fig.5(d)	100	Al
2 in Fig.5(d)	62.1	23.1	11.7	1.3	1.8	Ti(Al,Si) ₃
1 in Fig.6(a)	99.8	0.2	Al
2 in Fig.6(a)	10.7	33.0	53.5	0.5	2.3	τ_2
1 in Fig.6(b)	100	Al
2 in Fig.6(b)	10.7	30.7	56.1	0.4	2.1	τ_2
1 in Fig.6(c)	99.7	0.3	Al
2 in Fig.6(c)	11.2	32.1	56.1	0.6	...	τ_2
3 in Fig.6(c)	57.0	23.7	16.4	1.1	1.8	Ti(Al,Si) ₃
1 in Fig.6(d)	100	Al
2 in Fig.6(d)	18.1	30.6	49.3	...	2.0	τ_2
3 in Fig.6(d)	60.7	23.3	13.7	0.7	1.6	Ti(Al,Si) ₃
4 in Fig.6(d)	51.3	30.8	14.8	1.1	2.0	Ti(Al,Si) ₂

the formation of a Ti(Al,Si)₃ layer beneath the Ti-Si layer after pack cementation silicide coatings on γ -TiAl and also considered this as a result of rejection of Al into the substrate.

After 12 h heat treatment as shown in Fig. 5(d), the microstructure of the coating changed greatly. Two different layers could be observed. The outer layer (position 1 in Fig. 5d, Table 2) was aluminum, and the inner τ_2 layer

was replaced by a newly formed Ti(Al,Si)₃ layer (position 2 in Fig. 5d, Table 2) according to the EDS analysis. In as-sprayed Al-12Si alloy coating, the amount of Si content was limited. With the formation of τ_2 layer, the amount of Si in original coating decreased. When Si was used up, the τ_2 layer stopped growing. Meanwhile, Al in original coating started to diffuse to substrate. With the inward diffusion of Al, τ_2 layer degraded.

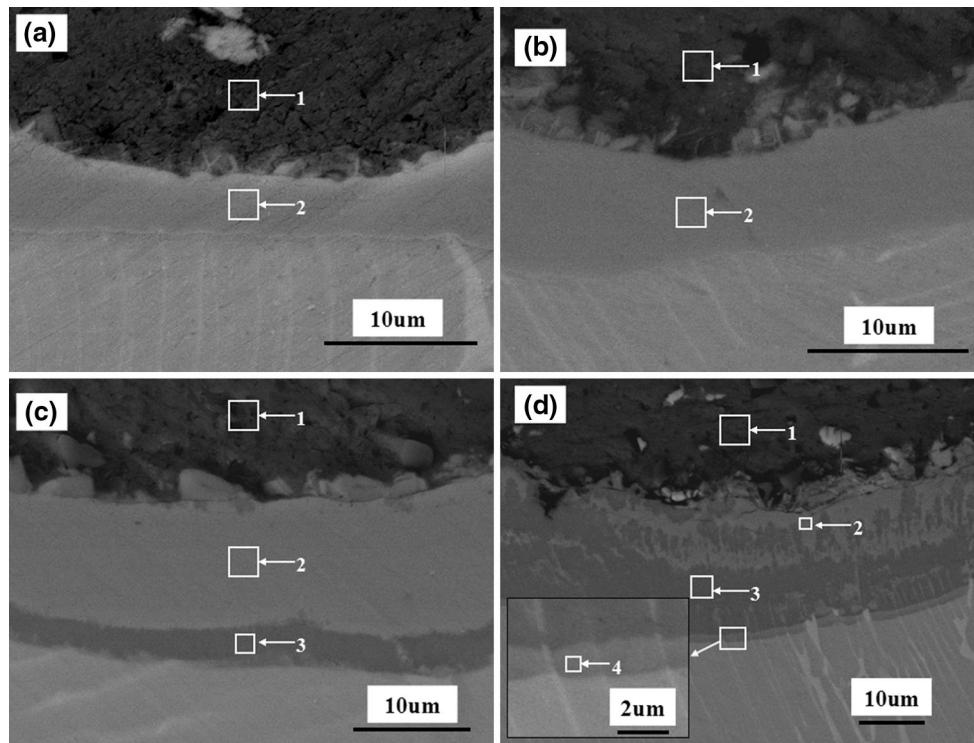


Fig. 6 Microstructure of the Al-20Si alloy coating after heat treatment at 580 °C for (a) 2 h, (b) 4 h, (c) 8 h, and (d) 12 h

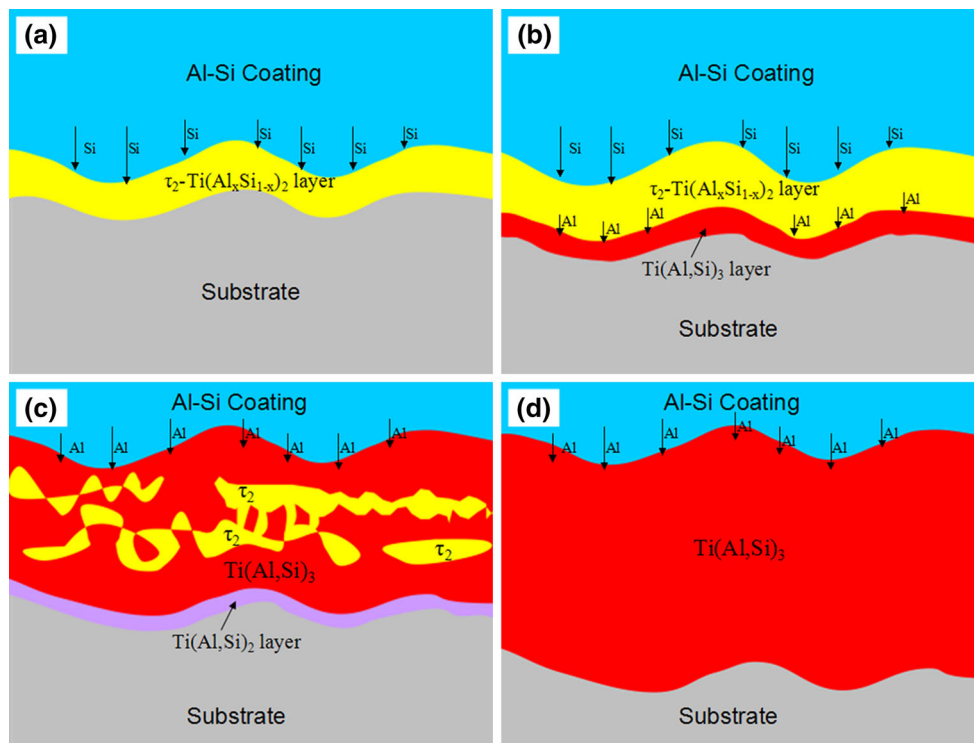


Fig. 7 Schematic diagram of the microstructure evolution of the Al-Si alloy coatings during heat treatment

Figure 6 shows the microstructure of Al-20Si alloy coating after heat treatment at 580 °C for 2, 4, 8, and 12 h. It could be seen that the microstructure of Al-20Si alloy coating after the heat treatment was similar to that of Al-12Si alloy coating. The difference was that the τ_2 layer of the former was thicker than the latter because of the higher Si content in Al-20Si alloy coating. Thus the τ_2 phase still coexisted with $\text{Ti}(\text{Al},\text{Si})_3$ after 12-h heat treatment as shown in Fig. 6(d). Besides the $\text{Ti}(\text{Al},\text{Si})_3$ and τ_2 phases, a 2 μm uniform layer was formed at the interface between the diffusion coating and the substrate. According to the EDS analysis (position 4 in Fig. 6d,

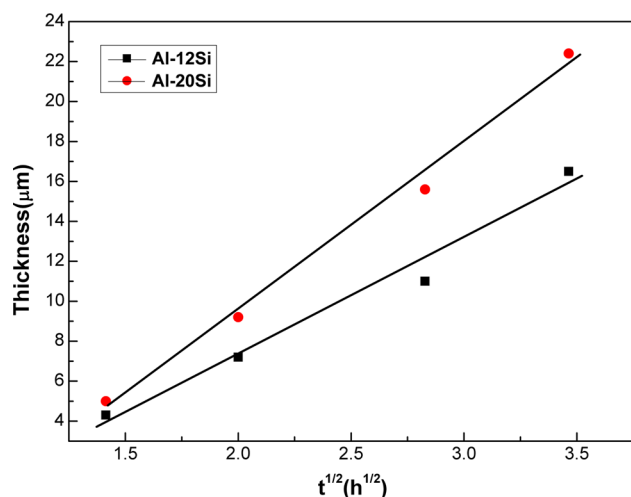


Fig. 8 Kinetics of the silicon-aluminizing coating at 580 °C

Table 3 EDS analysis of different positions in Fig. 9

Position	Al (at.%)	Ti (at.%)	Si (at.%)	Cr (at.%)	Nb (at.%)	Phase
1	98.9	1.1	Al
2	68.9	24.1	6.1	0.9	...	$\text{Ti}(\text{Al},\text{Si})_3$
3	100	Al
4	64.0	25.3	10.4	0.3	...	$\text{Ti}(\text{Al},\text{Si})_3$

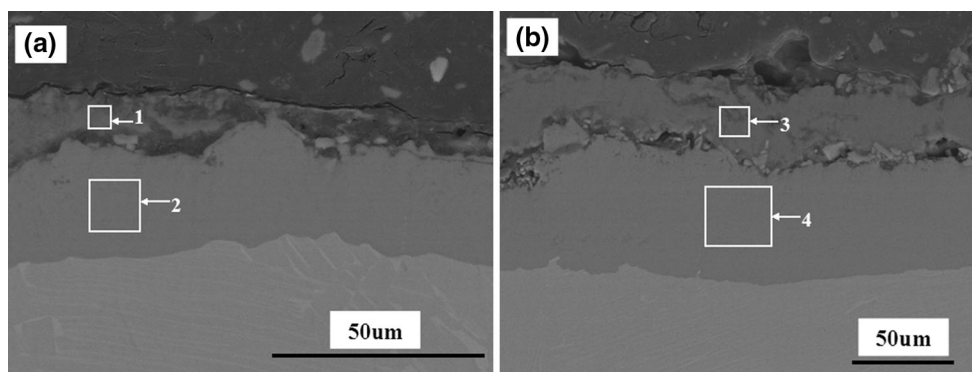


Fig. 9 Microstructure of the (a) Al-12Si and (b) Al-20Si alloy coatings after heat treatment at 650 °C for 12 h

Table 2), it might be that the Al atoms of $\text{Ti}(\text{Al},\text{Si})_2$ were partially substituted by Si atoms in TiAl_2 , which resulted from the interdiffusion between the $\text{Ti}(\text{Al},\text{Si})_3$ and $\gamma\text{-TiAl}$ substrate.

Figure 7 shows the schematic diagram of the microstructure evolution of Al-Si alloy coatings during heat-treatment process. At the first stage, Si strongly diffused into substrate and reacted with TiAl , which resulted in the formation of $\tau_2\text{-Ti}(\text{Al}_x\text{Si}_{1-x})_2$ layer. With the formation of τ_2 layer, the excess Al in original TiAl phase was rejected into the substrate and was accumulated under τ_2 layer, which resulted in the formation of $\text{Ti}(\text{Al},\text{Si})_3$ layer. At the second stage, the τ_2 phase degraded with the increase of the inward diffusion of Al. Finally, the τ_2 phase was consumed totally and a sole $\text{Ti}(\text{Al},\text{Si})_3$ diffusion coating was formed on the substrate.

According to the aforementioned analysis, both Si and Al diffused into $\gamma\text{-TiAl}$ substrate. Therefore, heat treating the cold-sprayed Al-Si alloy coatings can be one of the silicon-aluminizing methods on $\gamma\text{-TiAl}$ substrate. This novel silicon-aluminizing method was firstly reported. Comparing to the conventional pack cementation method, it is more convenient and environmentally friendly because there is no need for the pack mixtures and activators. Furthermore, during the heat-treatment process, it was found that Si was the first inward diffusion element rather than Al because τ_2 layer with high Si content was the firstly formed compound. The formation of $\text{Ti}(\text{Al},\text{Si})_3$ layer as shown in Fig. 5(c) and (d) further demonstrated this point. Although thermodynamics indicates that combining capability of Si with Ti is much stronger than that of Al with Ti (Ref 17), the formation of τ_2 layer is the direct experimental evidence that Si has a greater affinity with Ti in the TiAl . This finding is significant for accurately con-

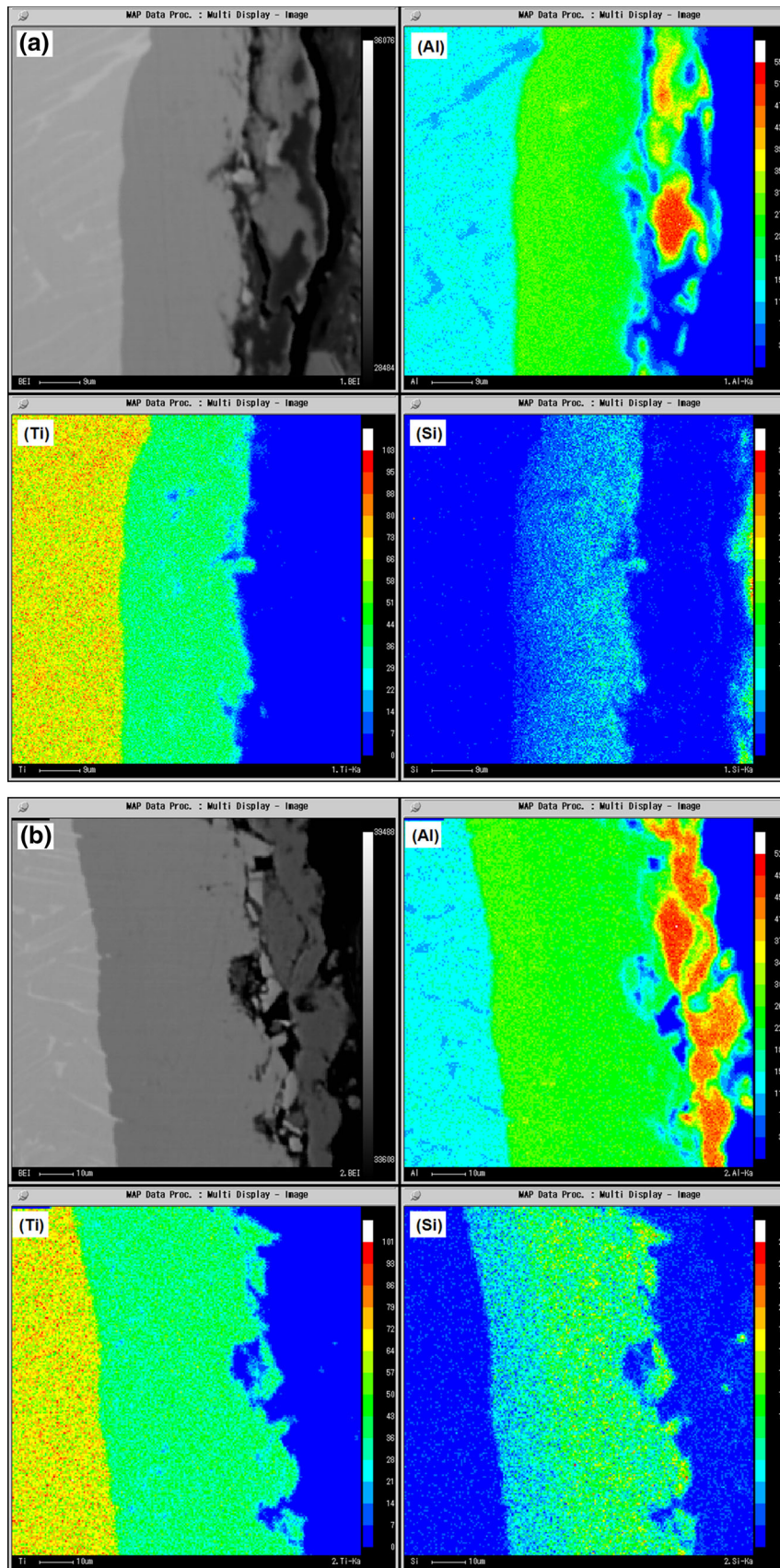


Fig. 10 MPMA elemental maps of the (a) Al-12Si and (b) Al-20Si alloy coatings after heat treatment at 650 °C for 12 h

control the amount of Si and Al in silicon-aluminizing coating on γ -TiAl substrate.

3.4 Kinetics of the Silicon-Aluminizing Coating at 580 °C

It was found that the thickness of the silicon-aluminizing coating increased with the increase in heat-treatment time. Thus the thickness of the silicon-aluminizing coating was plotted as a function of the square root of the heat-treatment time, as presented in Fig. 8. It could be seen that the thickness of the coating increased linearly with the increasing square root of the heat-treatment time. The increase in the thickness of the coating can be described as $y = kt^{1/2} + b$, in which y is the thickness, k is the parabolic rate constant, t is the heat-treatment time, and b is an offset value induced by the heating and cooling processes. According to the calculation, the k value of the Al-12Si alloy coating is $6 \mu\text{m}/\text{h}^{1/2}$ and that of the Al-20Si alloy coating is $8 \mu\text{m}/\text{h}^{1/2}$. It indicated that the thickness of the Al-20Si alloy coating increased more quickly than that of the Al-12Si alloy coating with the heat-treatment time.

3.5 Microstructure of the Silicon-Aluminizing Coating After Heat Treatment at 650 °C

The thickness of the silicon-aluminizing coating after heat treatment at 580 °C for 12 h was about 20 μm . To get a thicker diffusion coating, a heat treatment at 650 °C was used. Figure 9 shows the microstructure of (a) Al-12Si and (b) Al-20Si alloy coatings after heat treatment at 650 °C for 12 h. Table 3 shows the EDS analysis. It could be seen that the thickness of the silicon-aluminizing coating after heat treatment at 650 °C for 12 h was higher than that after heat treatment at 580 °C for 12 h because the inward diffusion velocity of Si and Al was faster at high temperature. It was more obvious for the Al-20Si diffusion coating whose thickness could reach up to 60 μm , 3 times as that after heat treatment at 580 °C for 12 h. The diffusion coating was also $\text{Ti}(\text{Al},\text{Si})_3$ according to the EDS analysis. The content of Si in the diffusion coating after heat treatment at 650 °C for 12 h (position 4 in Fig. 8b, Table 3) was slightly less than that after heat treatment at 580 °C for 12 h because of the dilution of the inward diffusion of Al. The gross amount of Si in the diffusion coating is constant. With the increase in the inward diffusion of Al, the proportion of Si in the diffusion coating decreases. In spite of the brittleness and low ductility of the TiAl_3 diffusion layer compared to TiAl substrate, no significant cracks in $\text{Ti}(\text{Al},\text{Si})_3$ coating were observed. It was probably because thin coatings were less prone to crack formation than thicker coatings, as it was reported in other studies (Ref 6, 29).

Figure 10 shows the EPMA elemental maps of Al, Ti, and Si of (a) Al-12Si and (b) Al-20Si coatings after heat treatment at 650 °C for 12 h. It could be seen that both Al and Si had diffused into the substrate. Furthermore, the distribution of Si was uniform without obvious elemental enrichment. It is widely reported that the TiAl_3 phase has good oxidation resistance (Ref 6-11). Therefore, it is

believed that the $\text{Ti}(\text{Al},\text{Si})_3$ coating can also improve the oxidation resistance of the bare alloy effectively. The oxidation behavior of this coating needs further study.

4. Conclusion

A novel silicon-aluminizing process was conducted on γ -TiAl substrate. The silicon-aluminizing process included two steps. In the first step, Al-12Si and Al-20Si alloy coatings were prepared on γ -TiAl by cold spray. The results indicated that the microstructure of the as-sprayed coatings was similar to that of the feedstock particles. In the second step, the as-sprayed coatings were subjected to heat treatment. During the heat treatment at 580 °C, a τ_2 layer with high Si content was firstly formed through the inward diffusion of Si element into the substrate. Then with the inward diffusion of aluminum, the τ_2 layer degraded and was replaced by a $\text{Ti}(\text{Al},\text{Si})_3$ layer. The kinetics curve of silicon-aluminizing coating at 580 °C similarly followed parabolic law. Improving the heat-treatment temperature could increase the diffusion velocity of Si and Al and thus get a thicker silicon-aluminizing coating. This silicon-aluminizing coating was compact and crack free. It has the potential to be used as an oxidation resistance coating on γ -TiAl substrate.

Acknowledgment

The financial support of National Natural Science Foundation of China (No. 50971127) is gratefully acknowledged.

References

1. F. Appel, U. Brossmann, U. Christoph, S. Eggert, P. Janschek, U. Lorenz, J. Mullauer, M. Oehring, and J.D.H. Paul, Recent Progress in the Development of Gamma Titanium Aluminide Alloys, *Adv. Eng. Mater.*, 2000, **2**(11), p 699-720
2. H. Clemens and H. Kestler, Processing and Applications of Intermetallic Gamma-TiAl-Based Alloys, *Adv. Eng. Mater.*, 2000, **2**(9), p 551-570
3. K. Kothari, R. Radhakrishnan, and N.M. Wereley, Advances in Gamma Titanium Aluminides and Their Manufacturing Techniques, *Prog. Aerosp. Sci.*, 2012, **55**, p 1-16
4. D. McKee and S. Huang, The Oxidation Behavior of Gamma-Titanium Aluminide Alloys Under Thermal Cycling Conditions, *Corros. Sci.*, 1992, **33**(12), p 1899-1914
5. M. Schmiedgen, P. Graat, B. Baretzky, and E. Mittemeijer, The Initial Stages of Oxidation of γ -TiAl: an X-ray Photoelectron Study, *Thin Solid Films.*, 2002, **415**(1), p 114-122
6. V. Gauthier, F. Dettenwanger, M. Schütze, V. Shemet, and W. Quadackers, Oxidation-Resistant Aluminide Coatings on γ -TiAl, *Oxid. Met.*, 2003, **59**(3-4), p 233-255
7. C.H. Koo and T.H. Yu, Pack Cementation Coatings on $\text{Ti}_3\text{Al-Nb}$ Alloys to Modify the High-Temperature Oxidation Properties, *Surf. Coat. Technol.*, 2000, **126**(2-3), p 171-180
8. M.S. Chu and S.K. Wu, The Improvement of High Temperature Oxidation of Ti-50Al by sputtering Al Film and Subsequent Interdiffusion Treatment, *Acta Mater.*, 2003, **51**(11), p 3109-3120
9. Z.G. Zhang, X. Teng, Y.L. Mao, C.X. Cao, S.J. Wang, and L. Wang, Improvement of Oxidation Resistance of γ -TiAl at 900

- and 1000 °C Through Hot-Dip Aluminizing, *Oxid. Met.*, 2009, **73**(12), p 455-466
10. L. Kong, B. Lu, X. Cui, H. Du, T. Li, and T. Xiong, Oxidation Behavior of TiAl₃/Al Composite Coating on Orthorhombic-Ti₂AlNb Based Alloy at Different Temperatures, *J. Therm. Spray Technol.*, 2010, **19**(3), p 650-656
 11. J.Q. Wang, L.Y. Kong, T.F. Li, and T.Y. Xiong, Oxidation Behavior of Thermal Barrier Coatings with a TiAl₃ Bond Coat on Gamma-TiAl Alloy, *J. Therm. Spray Technol.*, 2015, **24**(3), p 467-475
 12. X.Y. Li, S. Taniguchi, Y.C. Zhu, K. Fujita, N. Iwamoto, Y. Matsunaga, and K. Nakagawa, Oxidation Behavior of TiAl Protected by Si Plus Nb Combined Ion Implantation, *Intermetallics.*, 2001, **9**(5), p 443-449
 13. S. Taniguchi, T. Kuwayama, Y.C. Zhu, Y. Matsumoto, and T. Shibata, Influence of Silicon Ion Implantation and Post-implantation Annealing on the Oxidation Behaviour of TiAl Under Thermal Cycle Conditions, *Mater. Sci. Eng. A-Struct.*, 2000, **277**(1-2), p 229-236
 14. T.C. Munro and B. Gleeson, The Deposition of Aluminide and Silicide Coatings on Gamma-TiAl using the Halide-Activated Pack Cementation Method, *Metall. Mater. Trans. A.*, 1996, **27**(12), p 3761-3772
 15. L. Swadzba, A. Maciejny, B. Mendala, G. Moskal, and G. Jarczyk, Structure and Resistance to Oxidation of an Al-Si Diffusion Coating Deposited by Arc-PVD on a TiAlCrNb Alloy, *Surf. Coat. Technol.*, 2003, **165**(3), p 273-280
 16. Z. Xiang, S. Rose, and P. Datta, Codeposition of Al and Si to Form Oxidation-Resistant Coatings on γ -TiAl by the Pack Cementation Process, *Mater. Chem. Phys.*, 2003, **80**(2), p 482-489
 17. H.P. Xiong, Y.H. Xie, W. Mao, W.L. Ma, Y.F. Chen, X.H. Li, and Y.Y. Cheng, Improvement in the Oxidation Resistance of the TiAl-Based Alloy by Liquid-Phase Siliconizing, *Scripta Mater.*, 2003, **49**(11), p 1117-1122
 18. H.P. Xiong, W. Mao, Y.H. Xie, W.L. Ma, Y.F. Chen, X.H. Li, J.P. Li, and Y.Y. Cheng, Liquid-Phase Siliconizing by Al-Si Alloys at the Surface of a TiAl-Based Alloy and Improvement in Oxidation Resistance, *Acta Mater.*, 2004, **52**(9), p 2605-2620
 19. H. Assadi, F. Gartner, T. Stoltenhoff, and H. Kreye, Bonding Mechanism in Cold Gas Spraying, *Acta Mater.*, 2003, **51**(15), p 4379-4394
 20. T.H. Van Steenkiste, J.R. Smith, and R.E. Teets, Aluminum Coatings via Kinetic Spray with Relatively Large Powder Particles, *Surf. Coat. Technol.*, 2002, **154**(2-3), p 237-252
 21. T. Stoltenhoff, H. Kreye, and H. Richter, An Analysis of the Cold Spray Process and Its Coatings, *J. Therm. Spray Technol.*, 2002, **11**(4), p 542-550
 22. J.L. Murray and A.J. McAlister, Phase-Diagrams for Industry-the Al-Si Binary, *Met. Prog.*, 1985, **128**(8), p 38
 23. W.Y. Li, C. Zhang, X.P. Guo, G. Zhang, H.L. Liao, and C. Coddet, Deposition Characteristics of Al-12Si Alloy Coating Fabricated by Cold Spraying with Relatively Large Powder Particles, *Appl. Surf. Sci.*, 2007, **253**(17), p 7124-7130
 24. D.H. Lu, Y.H. Jiang, G.S. Guan, R.F. Zhou, Z.H. Li, and R. Zhou, Refinement of Primary Si in Hypereutectic Al-Si Alloy by Electromagnetic Stirring, *J. Mater. Process. Technol.*, 2007, **189**(1-3), p 13-18
 25. Y.S. Tao, T.Y. Xiong, C. Sun, H.Z. Jin, H. Du, and T.F. Li, Effect of Alpha-Al₂O₃ on the Properties of Cold Sprayed Al/alpha-Al₂O₃ Composite Coatings on AZ91D Magnesium Alloy, *Appl. Surf. Sci.*, 2009, **256**(1), p 261-266
 26. S.P. Gupta, Intermetallic Compounds in Diffusion Couples of Ti with an Al-Si Eutectic Alloy, *Mater. Charact.*, 2002, **49**(4), p 321-330
 27. O. Dezellus, B. Gardiola, J. Andrieux, M. Lomello-Tafin, and J.C. Viala, On the Liquid/Solid Phase Equilibria in the Al-Rich Corner of the Al-Si-Ti Ternary System, *J. Phase. Equilib. Diff.*, 2014, **35**(2), p 137-145
 28. H.P. Xiong, Q. Shen, J.G. Li, L.M. Zhang, and R.Z. Yuan, Design and Microstructures of Ti/TiAl/Al System Functionally Graded Material, *J. Mater. Sci. Lett.*, 2000, **19**(11), p 989-993
 29. T.C. Munro and B. Gleeson, The Deposition and Oxidation Resistance of Aluminide Coatings on γ -TiAl, *Mater. Sci. Forum.*, 1997, **753**(251-254), p 753-760